Available online at www.sciencedirect.com
ScienceDirect
Acta Biomaterialia 4 (2008) 1089–1094
Acta BIOMATERIALIA
www.elsevier.com/locate/actabiomat

Energy dispersive X-ray diffraction study of phase development during hardening of calcium phosphate bone cements with addition of chitosan

J.V. Rau [a], A. Generosi [b], V.V. Smirnov [c], D. Ferro [a], V. Rossi Albertini [b], S.M. Barinov [c,*]

[a] *Istituto per lo Studio dei Materiali Nanostrutturati, CNR, Piazzale Aldo Moro, 5-0185 Rome, Italy*
[b] *Istituto di Struttura della Materia, CNR, Via del Fosso del Cavaliere, 100-00133 Rome, Italy*
[c] *Institute for Physical Chemistry of Ceramics, Russian Academy of Sciences, Ozernaya, 48-119361 Moscow, Russia*

Received 26 September 2007; received in revised form 4 December 2007; accepted 10 January 2008
Available online 26 January 2008

Abstract

The aim of this work was to study the phase transformation during the setting reaction of two calcium phosphate bone cements based on either alpha tricalcium phosphate (α-TCP) or tetracalcium phosphate (TetCP) initial solid phase, and a magnesium carbonate–phosphoric acid solution as the hardening liquid. Low molecular weight (38.2 kDa) chitosan was used to retard the cement's setting reaction. To follow the kinetics of the phase development, an energy dispersive X-ray diffraction technique was applied. This technique allowed the collection of diffraction patterns from the cement pastes in situ starting from 1 min of the setting process. In the case of the TetCP-based cement, the appearance and evolution of an intermediate phase was detected.

Keywords: Calcium phosphate bone cements; Chitosan; Phase transformations; X-ray diffraction

1. Introduction

Calcium phosphate bone cements (CPC) are self-setting biocompatible materials which have been developed for medical applications to restore damaged human calcified tissue [1–6]. The most recent achievements and new trends in the field of CPC materials have been reviewed by Bohner et al. [5]. CPC consists of one or more calcium phosphate powders and a hardening liquid. If the powder and the liquid are mixed, they form a paste that can be moulded to the shape of a bone defect and set fast by entanglement of the crystals within the paste. The final products of the setting reaction may be dicalcium phosphate dihydrate (DCPD), precipitated hydroxyapatite or a mixture of the two. The properties of CPC can be affected by the composition of both the powder and the liquid constituents, the powder-to-liquid ratio, and additional biocompatible components, e.g., biopolymers such as gelatin and chitosan, the latter being biologically renewable, biodegradable, biocompatible and biofunctional [7].

Despite the relatively long history of CPC, little is known at present about some of their basic properties, such as the setting behaviour and hardening mechanism [4,8]. It was demonstrated in a previous study that the phase development process during the primary crystallization is very fast [9]. Apatite crystallization is completed within a few seconds of the setting reaction followed by secondary crystallization with characteristic times ~23 and 16 h for the cements composed of alpha tricalcium phosphate (α-TCP) and tetracalcium phosphate (TetCP) powders, respectively, and with Mg-containing phosphoric acid as the hardening liquid [9].

A number of studies have been devoted to the effect of gelatin and chitosan on the CPC properties [10–15]. Chitosan is known to inhibit the hydroxyapatite precipitation

* Corresponding author. Tel.: +7 495 4379892; fax: +7 495 4379893.
E-mail address: barinov_s@mail.ru (S.M. Barinov).

1742-7061/$ - see front matter © 2008 Acta Materialia Inc. Published by Elsevier Ltd. All rights reserved.
doi:10.1016/j.actbio.2008.01.006

[15]. The common methods of phase identification are too slow to monitor the phase composition changes within a few minutes of acquisition time. An energy dispersive X-ray diffraction (EDXD) method applied in this work allows the rapid collection of diffraction patterns, because it is carried out electronically rather than mechanically as in conventional (i.e., angular dispersive) X-ray diffraction. The present work involves the EDXD study of the phase development during the setting process in two different calcium phosphate cements (based on α-TCP and TetCP, respectively) affected by the addition of chitosan.

2. Materials and methods

Two different CPC were prepared. Cement 1 is based on α-TCP ($Ca_3(PO_4)_2$, Ca/P = 1.5) powder. The tricalcium phosphate was obtained as the precipitation product of the following reaction:

$$3Ca(NO_3)_2 + 2(NH_4)_2HPO_4 + 2NH_4OH + nH_2O \rightarrow Ca_3(PO_4)_2 \times nH_2O + 6NH_4NO_3 + 2H_2O \quad (1)$$

Analytical grade starting reagents were used. The solution pH was adjusted to 7 by adding solutions of acetic acid and ammonia. The solution with the precipitate was aged for 24 h, followed by filtering with a Buechner cone filter. After the calcinations of the precipitate in an air atmosphere furnace at 1300 °C for 1 h, monophasic α-TCP powder was obtained, as established by X-ray diffraction (XRD) analysis (Shimadzu XRD-6000 diffractometer, Cu $K_{\alpha 1}$ radiation, JCPDS data base). The powders were milled to the mean particle size of 10 ± 2 μm, measured using an optical microscopy (sample size 100 particles, Neophot-32 Carl Zeiss microscope).

Cement 2 was based on tetracalcium phosphate (TetCP, $Ca_4P_2O_9$) (Ca/P = 2) powder. The initial reagents, calcium oxide and solid ammonium hydrophosphate, were mixed in a planetary ball mill for 30 min using alumina balls. After that, the mix was heat treated at 1500 °C for 1 h in an air furnace to initiate the following reaction:

$$4CaO + 2(NH_4)_2HPO_4 \rightarrow Ca_4P_2O_9 + NH_3 + 3NH_4OH \quad (2)$$

The reaction product, a white powder, was milled in a ball mill to the mean particle size of ~10 μm. XRD analysis showed that the powder was TetCP containing a minor amount of hydroxyapatite (about 3 wt.%, determined using a calibration curve) as an impurity phase.

To obtain the cement pastes, two liquids were prepared by the following methods. Liquid 1 for cement 1 was prepared by mixing 0.15 g of magnesium carbonate, $MgCO_3$, with 0.18 ml of 30 wt.% H_3PO_4 acid. The same procedure was employed for cement 2, but with 0.22 ml of acid (liquid 2). Magnesium carbonate reacts with phosphoric acid, the reaction product being an aqueous solution of magnesium phosphate of various Mg/PO_4 ratios, depending on the initial reagents ratio.

The chitosan-containing mixtures were prepared by adding 0.02 g, 0.01 g and 0.001 g of a water-soluble chitosan (low molecular weight (38.2 kDA), 75% deacetylated chitosan supplied by Aldrich Chemical Co.) to every hardening liquid (0.25 ml) followed by intensive mixing for 1 min until homogeneous mixtures were formed. Then the precursor powder (α-TCP or TetCP (0.2 g)) was added to the mixtures based on liquid 1 and liquid 2, respectively, and mixed again for 1 min until a cream-like paste was formed.

Subsequently, the resulting structural modifications were monitored in real time, collecting sequences of diffraction patterns. The acquisition time of each pattern was set at 60 s and the overall observation time was 72 h.

The EDXD measurements were performed by a non commercial apparatus, based on the use of a non-monochromatized ('white') primary X-ray beam (produced by a W anode (12–55 keV)) and an ultra pure Ge solid-state detector, which is able not only to count the number of diffracted photons but also to measure the energy of each of them. In this way, the reciprocal space scan necessary to construct the diffraction pattern, i.e., the scan of the scattering parameter q (where $q = aE\sin\vartheta$ is the normalized momentum transfer magnitude; a is a constant, E is the energy of the incident X-ray beam, and 2ϑ is the scattering angle), is carried out electronically [16,17].

The main advantage of the energy dispersive mode over its conventional counterpart in performing X-ray diffraction experiments is that the geometric set-up is kept fixed during the acquisition of the diffraction patterns, which simplifies the experimental geometry and prevents systematic angular errors as well as possible misalignments. In particular, the technique provides faster recording of the Bragg peaks as, in the ED mode, the whole diffraction pattern is obtained in parallel at any q value.

Prior to the real-time measurements, diffraction patterns of all components were collected ex situ (the optimal

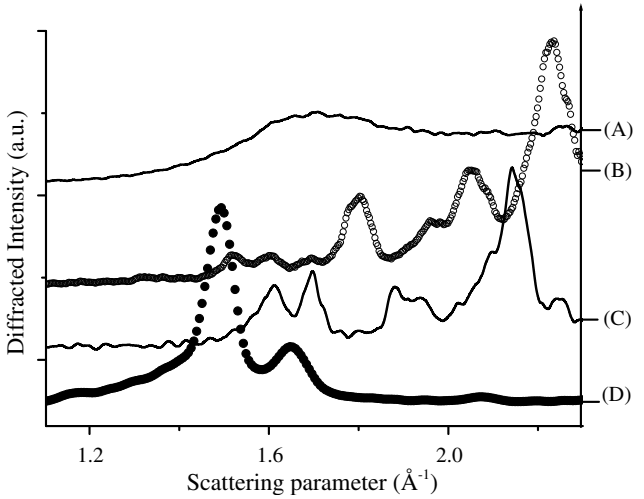

Fig. 1. Diffraction patterns of (A) chitosan, (B) $Ca_4P_2O_9$ powder, (C) α-$Ca_3(PO_4)_2$ powder and (D) $Ca_{10}(PO_4)_6(OH)_2$ final cement obtained without adding chitosan.

conditions found being $\vartheta = 2.671°$, $E = 55$ keV) and compared, as shown in Fig. 1. In the selected q range, each Bragg reflection could be easily assigned either to the precursor powders (B, C) or to the final cement (D), no confusion being possible because the peaks are well separated. The diffraction signal produced by pure chitosan (A) is very weak and appears as an X-ray amorphous diffuse halo. After this preliminary characterization, in situ EDXD studies were performed under the same experimental conditions.

Morphological investigation of the cement samples was performed using a scanning electron microscope (LEO 1450 VP) coupled with an INCA X-ray energy dispersive system (EDS). The samples were sputter-coated with gold prior to examination.

3. Results and discussion

In situ time-resolved EDXD measurements were carried out to study the crystallization process of hydroxyapatite, $Ca_{10}(PO_4)_6(OH)_2$ (hexagonal lattice, space group $P6_3/m$), obtained from two different precursor powders: α-TCP and TetCP.

In a previous work [9], the EDXD technique proved to be a suitable tool for observing the formation of the final hydroxyapatite phase starting from the same precursors, but the dynamics of the primary phase development was too fast (a few seconds) to be followed.

In the present work, to decrease the rate of the process, different quantities of chitosan were added to the hardening liquid, which was subsequently mixed with either α-TCP or TetCP. Since the presence of any quantity of chitosan does not alter the final product (hydroxyapatite), the only effect was an increase in crystallization times, which allowed the evolution from the starting reagents to the product to be followed in real time.

3.1. Precursor powder: α-TCP

The whole phase development process may be divided into two stages, the first of which corresponds to the formation of the primary product phase, and the other to a secondary slower rearrangement of this product, finally resulting in its hardening and consolidation.

In Fig. 2, the diffraction patterns of the α-TCP precursor powder, of the $Ca_{10}(PO_4)_6(OH)_2$ final product and of the primary product obtained adding 0.001 g of chitosan are shown. The primary product corresponds to $Ca_{10}(PO_4)_6(OH)_2$ (full dots), only the most intense [200] Bragg peak being detectable. No contribution of the initial α-TCP crystalline structure is visible and no secondary crystallization is observed afterwards, as evidenced by the constant intensity of the [200] peak over time (see the inset in Fig. 2, where the sequence of patterns collected during the hardening period, as a function of time, is present).

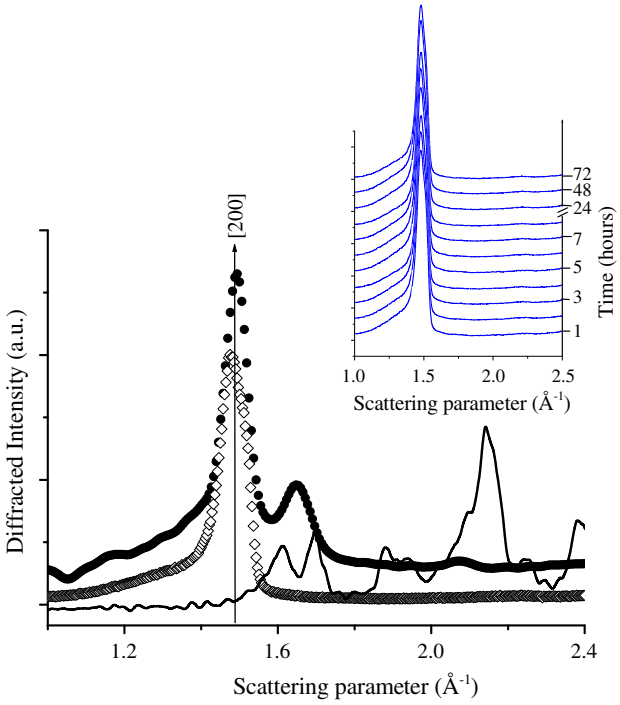

Fig. 2. Diffraction patterns of the α-TCP precursor powder (line), of the $Ca_{10}(PO_4)_6(OH)_2$ final product (full dots) and of the primary product (empty squares), obtained by the addition of 0.001 g chitosan. The inset shows the sequence of patterns collected during the hardening period as a function of time.

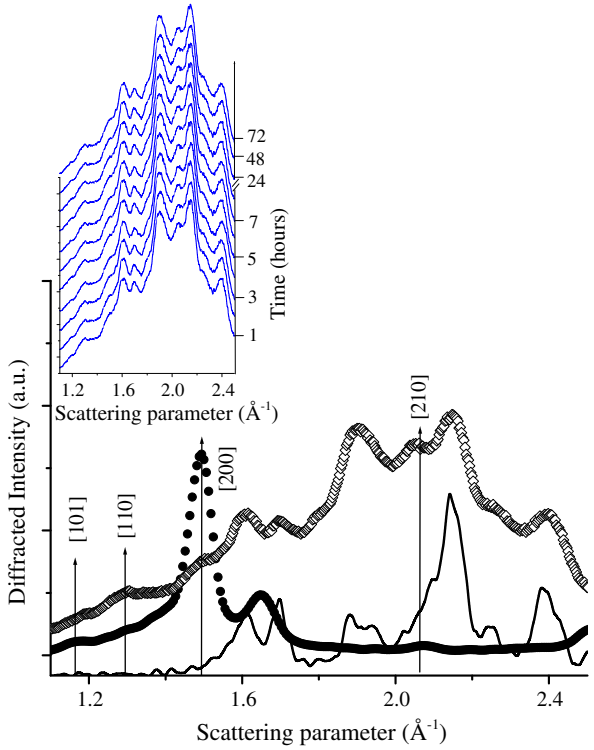

Fig. 3. Diffraction patterns of the α-TCP precursor powder (line), of $Ca_{10}(PO_4)_6(OH)_2$ (full dots) and of the primary product (empty squares) obtained by the addition of 0.02 g chitosan. The inset shows the time evolution of the diffraction patterns. Arrows indicate the peaks corresponding to the hydroxyapatite, the remaining peaks correspond to the α-TCP crystalline structure.

When 0.02 g of chitosan are added (see Fig. 3), the diffraction pattern of the primary product consists of Bragg reflections of both hydroxyapatite and α-TCP. Indeed, comparing the diffraction patterns of these compounds with the spectra of the primary product, it is evident that the latter is characterized by peaks arising from both $Ca_{10}(PO_4)_6(OH)_2$, and α-TCP. This indicates that the conversion of the initial mixture into hydroxyapatite is not complete, being partially inhibited by the relatively large amount of chitosan. The fraction of the precursor powder that did not turn into the primary product is considerable, as can be deduced from the ratio between $Ca_{10}(PO_4)_6(OH)_2$ and α-TCP peak intensity. Furthermore, the primary process is still too fast to be detected (a few seconds), no further structural modification occurring during the time subsequent to the primary crystallization, as evidenced by the analysis of the sequence of diffraction patterns collected over 72 h (see inset in Fig. 3).

Finally, 0.01 g of chitosan are added to the initial components, following the same experimental procedure. Also in this case, only a partial conversion of the α-TCP into $Ca_{10}(PO_4)_6(OH)_2$ was observed. However, a much larger amount of the initial mixture is converted into hydroxyapatite, as can be seen in Fig. 4, by comparing the diffraction patterns of different primary products. Indeed, in the present case, some of the initial features assigned to α-TCP are no longer present in the diffraction pattern of the primary product. Moreover, looking at the structural characteristics of hydroxyapatite, the primary product obtained by adding 0.01 g of chitosan still exhibits the same reflections, although their relative intensities differ from those of the initial compound (the [101], [110] and [210] reflections are the strongest, while the [200] peak is weak). This indicates that the amount of chitosan affects the transformation mechanism. It has also being possible to monitor the primary phase formation process following the evolution of the hydroxyapatite peaks. Visible in Fig. 5, both the [101] and [200] Bragg reflections (representative of the whole set of $Ca_{10}(PO_4)_6(OH)_2$ Bragg peaks) exhibit a similar time evolution, their relative intensities increasing up to a maximum value and then decreasing until a plateau is reached. By the Gaussian fit (line) of these time evolutions, the characteristic phase formation times were deduced ($\tau_{[101]} = (0.42 \pm 0.05)$ h, $\tau_{[200]} = (0.50 \pm 0.05)$ h, respectively), being fully consistent with each other. Moreover, the saturation is attained after (0.75 ± 0.05) h, which can be regarded as the overall time of the phase formation.

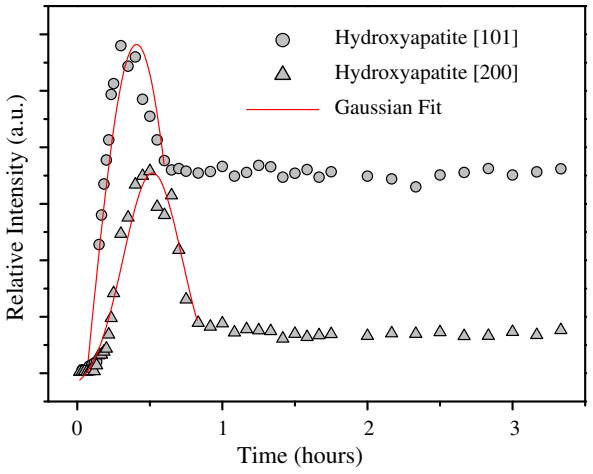

Fig. 5. Gaussian fit (line) of time evolution of the relative intensities of the hydroxyapatite [101] (dots) and [200] (triangles) Bragg reflections.

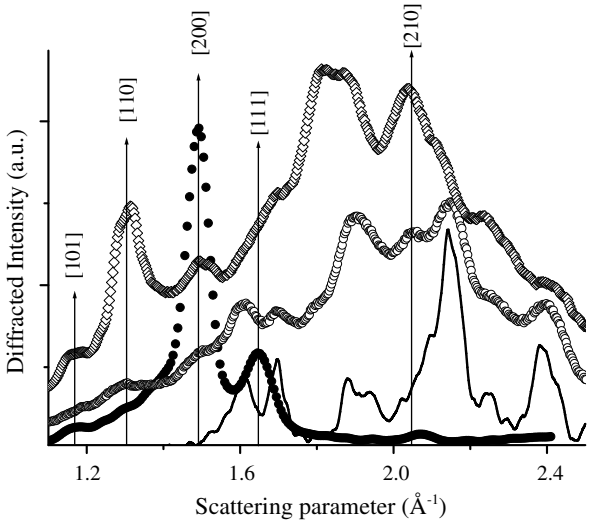

Fig. 4. Diffraction patterns of the α-TCP precursor powder (line), of $Ca_{10}(PO_4)_6(OH)_2$ (full dots), and of the primary products obtained adding 0.02 g (empty dots) and 0.01 g (empty squares) chitosan. Arrows indicate the peaks corresponding to the hydroxyapatite; the remaining peaks can be assigned to the α-TCP crystalline structure.

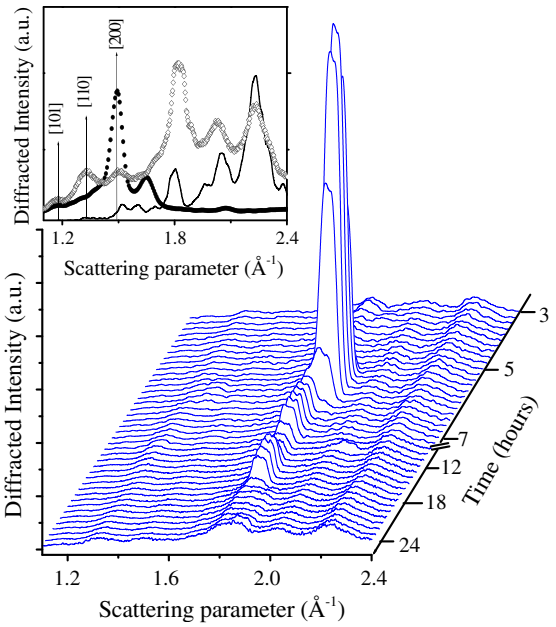

Fig. 6. Sequence of diffraction patterns collected as a function of setting time of the TetCP precursor powder with 0.02 g chitosan addition. In the inset, the initial components (line), the $Ca_{10}(PO_4)_6(OH)_2$ final cement (full dots) and primary products diffraction patterns (empty squares) are plotted for comparison.

3.2. Precursor powder: TetCP

When 0.001 g of chitosan are added, the $Ca_{10}(PO_4)_6(OH)_2$ primary cement ([200] oriented) is obtained, the transition time (a few seconds) being comparable with that of the process shown in Fig. 2, in which the α-TCP precursor powder has been used. However, the phase development processes with addition of 0.02 g and 0.01 g of chitosan is different. The sequence of diffraction patterns collected as a function of the setting time of the TetCP precursor powder with the addition of 0.02 g chitosan is shown in Fig. 6. Between the 5th and the 18th setting hour, an intermediate phase transition takes place, corresponding to the formation of the $CaHPO_4$ metastable phase with [200] and [003/022] reflections. It should be noted that a similar sequence of diffraction patterns was obtained in both cases (0.02 g and 0.01 g addition of chitosan). In both these cases, thanks to the in situ time-resolved EDXD measurements, it was possible to follow the evolution of various crystalline reflections. An intermediate phase transition occurs during the hardening period, with the formation and successive disappearance of $CaHPO_4$ (monetite, triclinic system, space group $P\bar{1}$ (2)) reflections. The formation of metastable monetite takes place according to the reaction (3) with the subsequent transformation into the hydroxyapatite

$$Ca_4P_2O_9 + 2H_3PO_4 \rightarrow 4CaHPO_4 + H_2O \quad (3)$$

In the inset in Fig. 6, a comparison between the initial components (line), the final cement (full dots) and the diffraction patterns of the primary products (empty squares) is presented. Such information could be obtained by ex situ measurements. However, from this analysis, it could be deduced only that the initial compound is partially converted into hydroxyapatite at the end of the primary process, and no hint of whether the transition involves intermediate metastable phases or not could be gained.

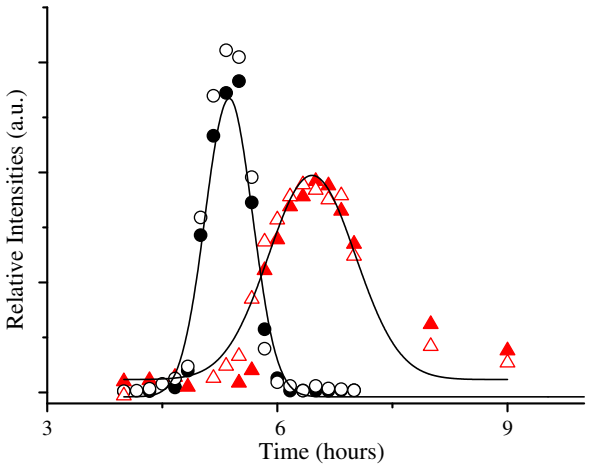

Fig. 7. Gaussian fit (line) of time evolution of the $CaHPO_4$ [200] (dots) and [003/022] (triangles) reflection intensities. It is visible that the phase transition occurs in the same characteristic time, regardless of the quantity of chitosan added (empty symbols, 0.01 g; full symbols, 0.02 g).

Instead, the accurate in situ monitoring of the hardening process time evolution revealed that two new Bragg reflections at $q = 1.420\ \text{Å}^{-1}$ and $q = 1.881\ \text{Å}^{-1}$, respectively, appear in the course of the reaction. These peaks correspond to the $CaHPO_4$ [003/022] and [200] orientations, their relative powder diffraction intensities being 15.5% and 100%, respectively. This phase transition is clearly visible on the sequences of diffraction patterns collected as a function of the scattering parameter and time (see Fig. 6). In Fig. 7, the time evolution of the $CaHPO_4$ [200] reflection intensity and of the [003/022] reflection intensity is shown. By an accurate Gaussian fitting (line) of each reflection, it is also possible to parameterize this intermediate transition by monitoring the intensity of both reflections as a function of the quantity of added chitosan and of time. As anticipated above, Fig. 7 demonstrates that the behaviour of the Bragg reflections is completely independent of the amount of chitosan. The transition characteristic times could be deduced and resulted to be $t_{[200]} = (5.50 \pm 0.25)$ h and $t_{[003/022]} = (6.25 \pm 0.25)$ h.

A SEM micrograph of the TetCP cement with 0.02 g addition of chitosan is shown in Fig. 8, the sample being set for 7 h. Large crystallites of up to 20 μm dimension can be seen. The EDS analysis revealed the Ca/P ratio to be equal to ~1:1. This result confirms the crystallized intermediate phase to be $CaHPO_4$, in agreement with the EDXD observation (Figs. 6 and 7).

To estimate the grain size from a diffraction pattern, the Scherrer formula is generally used. It can be calculated by writing the interference condition in correspondence of points P_1 and P_2 at the sides of a diffraction peak, where the intensity approaches zero, i.e., $2d \sin\vartheta_1 = (n+1)\lambda$ and $2d \sin\vartheta_2 = (n-1)\lambda$, where d is the average grain diameter, $\vartheta_1(\vartheta_2)$ is the angle corresponding to the left (right) side point $P_1(P_2)$, n is the order of the destructive interference (the counterpart of the nth order constructive interference, which produces the nth diffraction peak), and λ is the radiation wavelength. From these two relations, by defining FWHM as the full width half maximum and ϑ as the average between ϑ_1 and ϑ_2, the well-known Scherrer formula $d = \lambda/(\text{FWHM}\cos\vartheta)$ is straightforwardly obtained in the approximation that FWHM is twice $(\vartheta_2 - \vartheta_1)$.

However, the Scherrer formula is thought to describe diffraction data collected using the angular dispersive method. This formula can be generalized also to interpret the diffraction data acquired by the energy dispersive technique. For this purpose, the Laue equations, equivalent to the previous couple of interference conditions, can be used. The result is a relation involving the scattering parameter q, rather than the diffraction angle $d(q_2 - q_1) = 4\pi$, where $q_1(q_2)$ is the scattering parameter value corresponding to the point $P_1(P_2)$, as before. In the same approximation discussed above, the FWHM is twice $q_2 - q_1$. Therefore, $d = 2\pi/\text{FWHM}$, which coincides with the Fourier relation between conjugated variables. The result of the fits of single diffraction peaks is that they do not exhibit any evident broadening due to the finite size effect. This means that

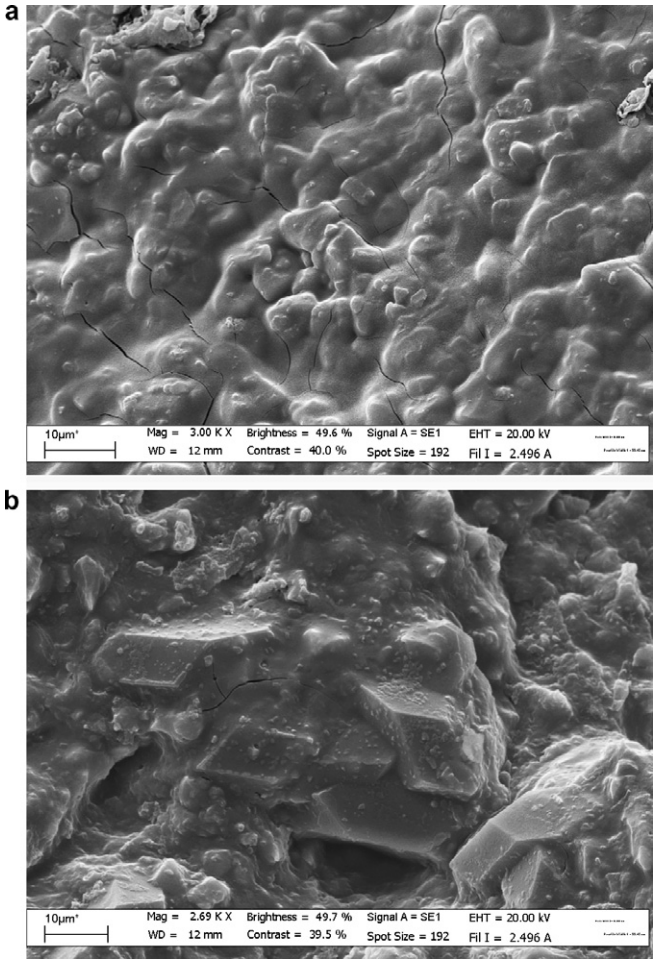

Fig. 8. SEM micrographs of (a) α-TCP cement and (b) TetCP cement after 7 h hardening period (0.02 g chitosan addition).

the average grain size is above the detection limit of the X-ray diffraction, i.e., a fraction of a micron or larger. This is in accordance with the SEM observation (Fig. 8).

Thus, the EDXD method allowed the in situ monitoring of the phase development in the CP cements containing chitosan. The addition of chitosan significantly influences the phase transformation during the setting and hardening processes in both the α-TCP- and the TetCP-based cements.

4. Conclusions

The phase development kinetics in both α-TCP and the TetCP cements were investigated by the EDXD method. The hardening process was inhibited by the addition of chitosan to the initial CPC mixture. In the case of the α-TCP precursor powder, the whole transformation process proceeded in two stages: the first (characteristic period 0.4–0.5 h) corresponded to the formation of a primary crystallization product, and the second- to a secondary slower rearrangement of this product, finally resulting in the cement hardening. The primary product of reaction was a blend of the initial α-TCP and the final $Ca_{10}(PO_4)_6(OH)_2$ phases. With a smaller amount (0.01 g) of chitosan, a much larger amount of the initial mixture was converted into the final hydroxyapatite phase. In the case of the TetCP precursor powder, the $CaHPO_4$ intermediate phase (characteristic period 5.5–6.3 h) was detected in the course of the hardening process. The evolution of the phase transition was independent of the amount of chitosan added (0.01–0.02 g).

Acknowledgements

This work is supported by the RAS-CNR agreement, project NT-14, and by the Russian Foundation for Basic Research, Grant No. 06-03-32192.

References

[1] LeGeros RZ, Chohayeb A, Shulman A. Apatitic calcium phosphates: possible dental restorative materials. J Dent Res 1982;61:343.
[2] Brown WE, Chow LC. A new calcium phosphate water-setting cement. In: Brown PW, editor. Cements research progress 1986. Berlin: Ohio, Westerville; 1987.
[3] Takagi S, Chow LC, Ishikawa K. Formation of hydroxyapatite in new calcium phosphate cements. Biomaterials 1998;19:1593–9.
[4] Fernandez E, Gil FJ, Ginebra MP, Driessens FCM, Planell JA, Best SM. Calcium phosphate bone cements for clinical applications. J Mater Sci Mater Med 1999;10:169–76.
[5] Bohner M, Gbureck U, Barralet JE. Technological issues for the development of more efficient calcium phosphate bone cements: a critical assessment. Biomaterials 2005;26:6423–9.
[6] Bohner M. Calcium orthophosphates in medicine: from ceramics to calcium phosphate cements. Injury 2000;31 S:37–47.
[7] Mayazaki S, Ishii K, Nadai T. The use of chitin and chitosan as drug carrier. Chem Pharm Bull (Tokyo) 1981;29:3067–9.
[8] Liu C, Shen W, Gu Y, Hu L. Mechanism of the hardening process for a hydroxyapatite cement. J Biomed Mater Res 1997;35:75–80.
[9] Generosi A, Smirnov VV, Rau JV, Rossi Alberini V, Ferro D, Barinov SM. Phase development in the hardening process of two calcium phosphate bone cements: an energy dispersive X-ray diffraction study. Mater Res Bull 2008;43:561–71.
[10] Fujishiro Y, Takahashi K, Sato T. Preparation and compressive strength of *a*-tricalcium phosphate/gelatin gel composite cement. J Biomed Mater Res 2001;54:525–30.
[11] Bigi A, Bracci B, Panzavolta S. Effect of added gelatin on the properties of calcium phosphate cement. Biomaterials 2004;25:2893–9.
[12] Maruyama M, Ito M. In vitro properties of a chitosan-bonded self-hardening paste with hydroxyapatite granules. J Biomed Mater Res 1996;32:527–32.
[13] Ito M, Miyazaki A, Yamagishi T, Yagasaki H, Hasem A, Oshida Y. Experimental development of a chitosan-bonded beta tricalcium phosphate bone filling paste. Biomed Mater Eng 1994;4:439–49.
[14] Liu H, Li H, Cheng W, Yang Y, Zhu M, Zhou C. Novel injectable calcium phosphate/chitosan composites for bone substitute materials. Acta Biomater 2006;2:557–65.
[15] Carey LE, Xu HHK, Simon Jr CG, Takagi S, Chow LC. Premixed rapid-setting calcium phosphate composites for bone repair. Biomaterials 2005;26:5002–14.
[16] Caminiti R, Rossi Alberini V. The kinetics of phase transition observed by energy dispersive x-ray diffraction. Int Rev Phys Chem 1999;18:263–99.
[17] Paci B, Generosi A, Rossi Alberini V, Agostinelli E, Varvaro G, Fiorani D. Structural and morphological characterization by energy dispersive X-ray diffractometry and reflectometry measurements of Cr/Pt bilayer films. Chem Mater 2004;16:292–8.